Measurement Science and Technology

PAPER • **OPEN ACCESS**

Metrological characterization methods for confocal chromatic line sensors and optical topography sensors

To cite this article: Jeremias Seppä *et al* 2018 *Meas. Sci. Technol.* **29** 054008

View the article online for updates and enhancements.

You may also like

- Calculation of high-frequency conductivity and Hall constant of a thin conductive layer in the view of equal specularity coefficients of its surfaces
  O V Savenko, I A Kuznetsova and A A Yushkanov
- On the application of the Ziman approximation for electrical conduction in thin films
  A M Ghodgaonkar and A D Tillu
- A physical interpretation of specularity parameter
  A M Ghodgaonkar, V N Bhoraskar and A D Tillu

This content was downloaded from IP address 202.8.112.197 on 06/07/2023 at 05:09

Measurement Science and Technology

Meas. Sci. Technol. **29** (2018) 054008 (10pp) https://doi.org/10.1088/1361-6501/aaad2b

Metrological characterization methods for confocal chromatic line sensors and optical topography sensors

Jeremias Seppä[1], **Karri Niemelä**[2] and **Antti Lassila**[1]

[1] VTT Technical Research Centre of Finland Ltd, Centre for Metrology MIKES, PO Box 1000, FI-02044 VTT, Finland
[2] Focalspec, Kaitoväylä 1, FI-90590 Oulu, Finland

E-mail: jeremias.seppa@vtt.fi

Received 21 December 2017, revised 29 January 2018
Accepted for publication 6 February 2018
Published 9 April 2018

Abstract
The increasing use of chromatic confocal technology for, e.g. fast, in-line optical topography, and measuring thickness, roughness and profiles implies a need for the characterization of various aspects of the sensors. Single-point, line and matrix versions of chromatic confocal technology, encoding depth information into wavelength, have been developed. Of these, line sensors are particularly suitable for in-line process measurement. Metrological characterization and development of practical methods for calibration and checking is needed for new optical methods and devices.

Compared to, e.g. tactile methods, optical topography measurement techniques have limitations related to light wavelength and coherence, optical properties of the sample including reflectivity, specularity, roughness and colour, and definition of optical versus mechanical surfaces.

In this work, metrological characterization methods for optical line sensors were developed for scale magnification and linearity, sensitivity to sample properties, and dynamic characteristics. An accurate depth scale calibration method using a single prototype groove depth sample was developed for a line sensor and validated with laser-interferometric sample tracking, attaining (sub)micrometre level or better than 0.1% scale accuracy. Furthermore, the effect of different surfaces and materials on the measurement and depth scale was studied, in particular slope angle, specularity and colour. In addition, dynamic performance, noise, lateral scale and resolution were measured using the developed methods.

In the case of the LCI1200 sensor used in this study, which has a 11.3 mm × 2.8 mm measurement range, the instrument depth scale was found to depend only minimally on sample colour, whereas measuring steeply sloped specular surfaces in the peripheral measurement area, in the worst case, caused a somewhat larger relative sample-dependent change (1%) in scale.

Keywords: optical sensors, calibration, metrology, optical scanners

(Some figures may appear in colour only in the online journal)

Original content from this work may be used under the terms of the Creative Commons Attribution 3.0 licence. Any further distribution of this work must maintain attribution to the author(s) and the title of the work, journal citation and DOI.

1. Introduction

The number of, and number of applications for, optical techniques for topography measurement in research and industrial production are steadily growing. The many benefits of optical topography include rapid measurement, non-contact probing of samples at multiple points simultaneously, stroboscopic capability and measurement of multiple layers. Application areas of such optical methods include in-line measurement of printed electronics and other highly parallel manufacturing processes, and rapid quality control of plastic parts or metal profiles.

A traceable length scale and realistic uncertainty estimates are needed in all dimensional measurements. Without traceability, measurement results are not repeatable or comparable with other results measured elsewhere, or even with those measured at different times or with different instruments at the same factory or laboratory. With high resolution and good repeatability of a modern quality instrument, the user easily forgets calibration and the absolute accuracy and traceability of the instrument scales. Some manufacturers, instead of giving measurement accuracy specifications, market only the resolution of their instruments. Traceable calibration, instrument stability and known metrological characteristics are all needed for reliable and accurate measurements.

Optical methods also have their drawbacks compared to, e.g. tactile probing. Possible issues include sensitivity to reflection coefficients, changes in specularly reflected versus scattered light intensity due to the surface finish or slope, and multiple reflection and propagation paths in the sample. Furthermore, the wavelength and coherence of the light used place limitations on performance. Speckle diffraction with coherent light can be exploited by some advanced surface texture methods [1], while with classical laser triangulation measurement it strongly limits the achievable performance, and methods with incoherent sources do not suffer from it.

Due to the growing demand for, and use of, e.g. confocal chromatic line-type sensors in, e.g. industrial control and fast non-tactile topography measurement, there is a need for feasible calibration methods and sensor characterization.

Various aspects of the calibration of optical surface topography instruments have been analysed by, e.g. Leach *et al* [1–3], including metrological characteristics (MCs) related to amplification, linearity, noise and resolution, and lateral squareness. In addition, e.g. the orthogonality of the depth axis to the lateral axes can be measured by, e.g. pyramidal shapes and error separation if needed [4, 5], and the lateral curvature of the profile line of line instruments can be determined.

The confocal chromatic principle is a group of optical methods increasingly used for, e.g. in-line optical topography measurement during industrial production. The principle has developed into various forms and instruments including point, line and matrix sensors [6–8]. The matrix versions tend to require some form of mechanical scanning. The chromatic confocal distance measurement principle is based on chromatic dispersion, focusing, spatial filtering and spectroscopy, and encoding depth information at different wavelengths. The classification of surface texture instruments, ISO 25178-6 2010, includes chromatic confocal probe instruments, described in the ISO document ISO 25178-602 2010 [9]. The effect of geometry and colour on certain point probes working with the chromatic principle has been characterized by Nouira [10].

In this article, an accurate depth scale calibration method using a single prototype groove depth sample is presented with the associated uncertainty analysis of groove depth measurement uncertainty, and the obtained Z calibration curve is compared to interferometric measurement. Methods are developed for the characterization of lateral scale and resolution, dynamic performance and vertical noise.

Finally, the effect of different surface types on the Z scale is characterized, in particular the slope angle, specularity and colour.

2. Selected metrological characteristics, optical sensor and setup

2.1. Terminology of the coordinate axes

In this article, the direction along the profile line is called X (X coordinate, variable x), the other 'lateral' direction, orthogonal to the profile line, is Y, and the chromatic 'depth' dimension, also often called the 'vertical' or 'axial' direction, is Z.

2.2. Metrological characteristics and properties selected for testing

The following MCs and properties were selected for this study:

- Scale:
  - Z scale amplification and linearity
  - X scale and resolution.
- Dynamic response and noise (Z).
- Probe-sample effects (Z):
  - Colour
  - Slope and specularity
  - Heterogeneous samples.

The selection was based on assumed and observed relevance to line chromatic sensors in particular. The main focus here is on Z scale magnification and linearity [2], and the effect of the sample properties on the Z scale, also including offset/flatness effects resulting from a heterogeneous sample. The dynamic behaviour and Z noise levels are also addressed.

2.3. Confocal chromatic line sensor

Several kinds of commercial line-type chromatic confocal sensors have been developed. Some of them, e.g. separate the optical signal from the sample to over a hundred optical fibres for analysis of separate lateral pixels. In this study we test the developed methods with an LCI1200 line confocal sensor, or lateral chromatic imaging sensor, by Focalspec. The LCI measurement head has a resolution of 2048 lateral pixels that are analysed first optically and then electronically inside the measurement head. The head is connected to a computer receiving the surface or interface point data analysed by the sensor head.

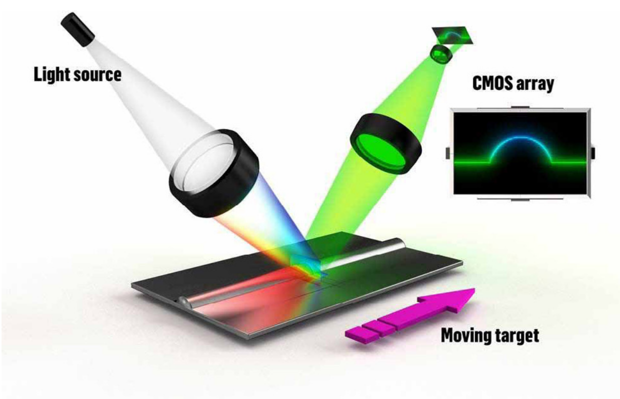

Figure 1. Illustration of the LCI line sensor principle. The height at each profile position is encoded into the wavelength of the detected light, which is measured as the position of a spectral peak for each lateral position by a matrix photodetector. Reproduced with permission from [11].

The working principle of LCI measurement is illustrated in figure 1. The detailed principles of the sensor are confidential, but the general principle is to shape the illuminating beam into a line, or vertical plane, where different wavelengths come into focus at different heights, and to read the scattered light with another optics unit at a roughly 90° angle to the illumination. The detection path detects only light that is in focus at each lateral position, and separates different wavelengths along the other axis of the matrix detector, resulting in a line profile. The Z resolution is at subpixel level, thanks to spectral peak fitting to the detected spectrum for each lateral position.

Almost any kind of surface can be measured with the LCI sensor. The nominal Z range of the LCI1200 instrument model used in this study is 2.80 mm and the X range is 11.26 mm. The LCI technology can optically measure snapshot profiles from surfaces and even multilayer interfaces with widely varying optical properties, at rates of up to thousands of profiles per second. For the LCI1200, the maximum nominal surface slope angle is 20° and the stand-off distance 16.16 mm. The nominal pixel size is 5.5 μm × 25 μm. Further specification is available on the manufacturer's website [11].

2.4. LCI sensor measurement setup with a laser interferometer

In order to establish a reference Z scale and allow sample movement and alignment, the LCI sensor was mounted on an optical table with the measured sample on a movable holder, and the Z movement of the sample was tracked with laser interferometry from the opposite side (back-to-back configuration). The setup is shown schematically in figure 2, and as an annotated photograph in figure 3. The setup allows motorized translation with low guidance errors/rotations, and the sample holder also has tilt angle adjustment up to 15°. The Z translation of the sample can be tracked accurately with laser interferometry traceable via the calibrated laser wavelength.

Alignment of the laser interferometer with the movement was done by driving the sample stage several centimetres and observing the returning laser beam from the cube corner reflector without the interferometer beamsplitter. The remaining cosine error angle was less than 0.5° based on the position stability of the returned beam. The Abbe offset between the centre of the LCI profile measurement line and the laser interferometer measurement axis (via the centre/apex of the cube corner reflector) was less than 2 mm.

The LCI was aligned with the sample stage Z movement by measuring sinusoidal topography gratings and with Ronchi rulers fixed to the sample stage in different orientations (grooves along X and Y, 100 μm grating pitch), so that the phase changes of the measured profiles when imaging the grating at different Z offsets correspond to less than 10 μm mm^{-1} of lateral displacement per Z displacement.

Guidance errors of the stage were characterized with an angle interferometry setting. The parasitic rotations corresponding to rotations around the X and Y axes amounted to a maximum change of $\pm 2''$ over 10 mm travel and $\pm 1''$ over 1 mm travel.

3. Calibration of the *Z* and *X* scales

3.1. Calibration of Z scale magnification and linearity with sample standard and with an interferometer

The most fundamental aspect of the length scale calibration is the scale magnification, and scale linearity. To develop an accurate and cost-efficient Z scale magnification and linearity calibration method, a method using a single standard sample was developed. The method based on a simple step height, or groove depth sample is applicable to *in situ* calibration of measurement instruments in an in-line factory measurement setting.

A prototype calibrated groove depth sample was constructed from three 1.1 mm-thick gauge blocks wrung together into an H shape, and measured at six different Z offsets at a roughly level orientation to the LCI. The measured LCI profiles and measurement areas from the groove sample are shown in figure 4.

For comparison, and in order to get a more detailed view on the scale, a Z scale calibration was also performed with laser interferometry, using a flat mirror target and comparing the Z scale of the LCI sensor at different parts of the X measurement range of the sensor to the laser interferometer, with the setup described earlier. The difference between the interferometric scale and LCI Z scale is shown in figure 5, each difference curve (each studied X interval) offset to zero mean difference between LCI and interferometer.

Table 1 shows the resulting values from the LCI measurement of the groove depth sample measurement values at the three locations, and the 'apparent sample height' calculated from them (before applying any scale correction).

A third-degree polynomial was fitted with the results shown in table 1, based on the following linear least-squares problem:

$$p_1\left(z_{i2} - \frac{1}{2}(z_{i1} + z_{i3})\right) + p_2\left(z_{i2}^2 - \frac{1}{2}(z_{i1}^2 + z_{i3}^2)\right) + p_3\left(z_{i2}^3 - \frac{1}{2}(z_{i1}^3 + z_{i3}^3)\right) = h_{\text{sample}}, \quad (1)$$

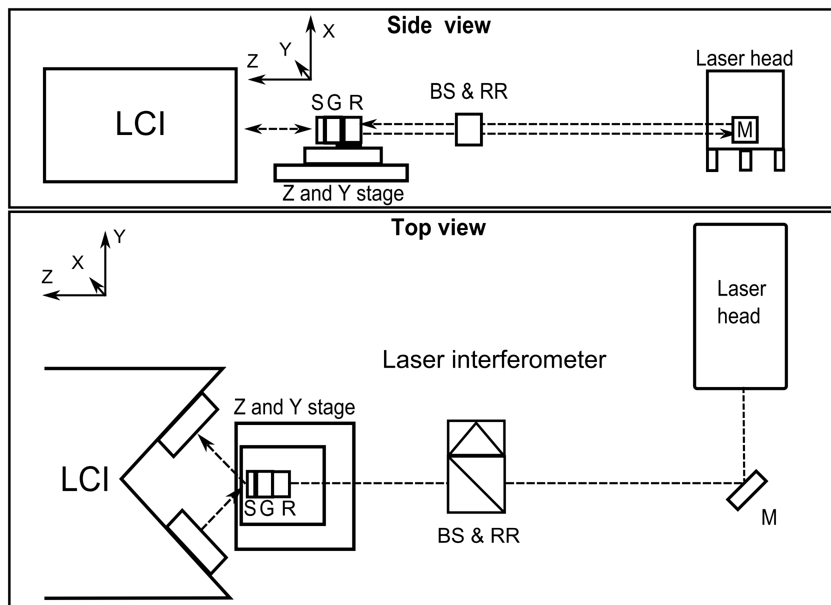

Figure 2. Setup for simultaneous LCI measurement and laser-interferometric z tracking. BS is the beamsplitter of the interferometer, G the goniometer stage, M the mirror, R the retroreflector (cube corner), RR the reference retroreflector and S is the sample. The laser head is a helium-neon heterodyne laser head (Agilent 5519A) also containing the interferometer photodetectors.

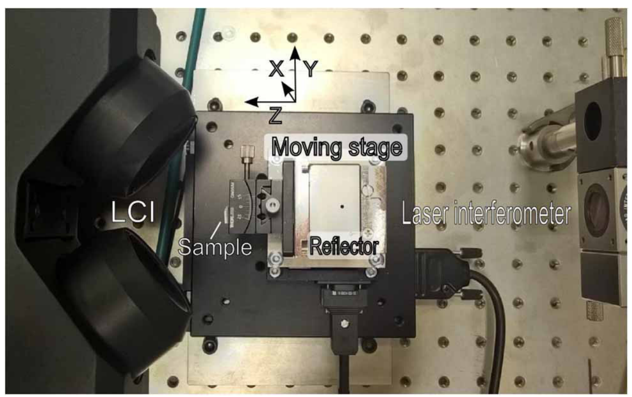

Figure 3. Photograph of the setup (top view).

where the height offset index i runs from 1 to 6 in this case. h_{sample} is the known height of the calibration sample prototype (1100 μm, uncertainty less than 0.1 μm) for all six equations. The solved parameters p_1–p_3 are the coefficients of the scaling and linearization polynomial (no zero-order offset here). The corresponding polynomial describing the scale error (or correction when inverted) is

$$p(z) = p_1 z + p_2 z^2 + p_3 z^3. \tag{2}$$

This is a third-degree polynomial describing the LCI Z scale obtained directly from the step height measurements with one step height sample. To get scale magnification, it is possible to fit just a first-degree polynomial instead of a higher degree, or just compare the known step height value to the value measured with LCI at Z scale areas of interest. (Using the p_1 coefficient from a higher order polynomial fit as the magnification does not work, due to the properties of the polynomial basis.) Using just one step height measurement without different offsets, however, gives no information about nonlinearity.

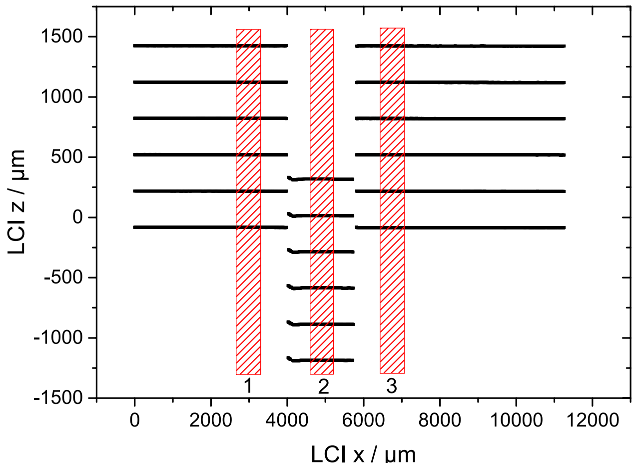

Figure 4. Groove depth sample prototype made of calibrated gauge blocks, measured at six different height offsets. X areas used for groove depth data analysis are denoted by the red numbered boxes.

The calibration function for the (average) Z scale obtained with the single step height sample is shown in figure 5, together with the interferometric results. Already, just by looking at figure 5, one can see that most of the Z scale has a magnification error of about 4 μm per 1 mm, or 0.4%, without correction.

The agreement of the results with these two methods is good, the full-scale results lying within 1 μm or less. The steel gauge blocks in the groove sample prototype also have a mirror-type highly specular surface, but with lower reflectivity.

The lower part of the figure (figure 5(b)) shows a central portion of the interferometrically measured Z scale, corrected by scaling with just one groove-depth measurement from the respective part of the scale. The accuracy of this part of the scale calibrated with a calibrated gauge block

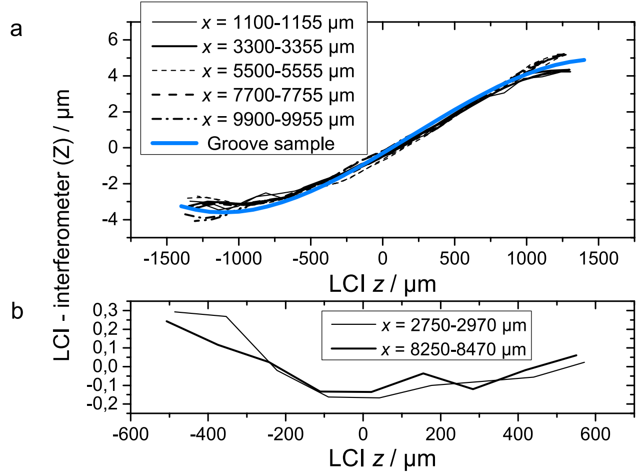

Figure 5. Interferometrically measured Z scale error of the LCI in different X areas (bidirectional scans) and polynomial fit (minus unity) from the groove depth sample measurements. (a) The zoomed middle part of the interferometrically measured scale error is also shown, after correcting the LCI Z scale amplification factor with one groove depth sample measurement. (b) Note the different scales. X-averaging areas are shown in the plot legends.

sample is of the order of 100 nm (interferometer—LCI, rms difference 0.14 μm).

Before the Z calibration, a flatness calibration and correction can be done by, e.g. measuring a level flat mirror in the central Z range to get a flat reference level for the Z offsets of different X-pixels. In the work presented here, this had already been done by the instrument manufacturer before the tests reported here.

The polynomial acquired using only one groove depth sample seems to agree well with the interferometrically measured LCI Z scale; in this sense, 'one step height is enough'. The alignment of the calibration sample angle with the LCI does not need to be very precise, and there is no need for precise evenly stepped Z offsets, as long as they cover the range of interest (somewhat evenly).

Based on the cosine nature of the tilt alignment errors, a 2.5° error in alignment (sample tilt angle) would only result in a relative error of slightly less than 0.1%. Also, the X-tilt can easily be compensated for, since it is seen in the measured profile. The Y-tilt can be minimized (and estimated) by measuring the sample with slightly differing Y-tilts and selecting that which corresponds to the smallest apparent step height. To realize the Z offsets, either the sample or the measuring instrument can be moved in the Z direction to change the working distance.

The ISO 5436-1:2000 [12] standard for step height and groove depth measurement, using line fitting to the areas, takes care of the X-tilt (sample rotation around Y). Here, however, the three similarly defined areas (symmetrical, or equidistant, middle third of the lower step used for calculation and similarly for the upper levels with the same margins to the edge as in the central part) are used by calculating the *average* z from each area, to make the least-squares fitting of a non-linear z scale function to make repeated groove measurements simpler to present.

Table 1. Groove depth sample measurement values.

Left z_1 (μm)	Middle z_2 (μm)	Right z_3 (μm)	Apparent groove depth h_{meas} (μm)
1468.41	362.58	1463.68	−1103.46
1168.03	60.84	1162.84	−1104.59
868.66	−239.24	863.00	−1105.08
566.82	−540.84	561.00	−1104.76
264.50	−842.48	258.95	−1104.20
−35.86	−1142.21	−41.48	−1103.54

An example measurement model and uncertainty budget was made based on the principles of GUM [13] for the step-height measurement. The model equation is

$$h = z_2 - \frac{1}{2}(z_1 + z_3) - \frac{\beta^2}{2}h_{nom} - \frac{\gamma^2}{2}h_{nom} - \Delta_{t20}\alpha h_{nom} - s - \delta_{rep}, \quad (3)$$

where z is the three measured heights from the areas at and next to the step (groove). The next two terms are small-angle approximations for the cosine errors due to the XY-tilt angles. β and γ are the angles in radians and h_{nom} is the nominal or approximate step height. Δ_{t20} is the sample temperature difference from 20 °C and α is the coefficient of thermal expansion of the sample. The refractive index changes of ambient air and/or instrument temperature sensitivity could be added, but here these (assumed almost negligible) effects are included in the repeatability.

s is the surface type and scale variation; in the case of a very small, constant surface slope (= level surfaces) and homogeneous optical surface properties, this error due to the surface affecting the scale is negligible. When measuring an unknown height with a calibrated chromatic instrument, a term for the residual uncertainty of the Z scale calibration could be added. When calibrating the z scale with a known sample this is not needed, and the measurement model reflects rather the uncertainty of the height presented to the instrument. The possible effects of the optical surface properties are analysed later in this paper. Variation of the Z scale as a function of x can also be included here (and could be included in the calibration model, based on gauge block measurements at multiple X offsets). δ_{rep} is the repeatability of the groove depth measurement. The three sample-area height uncertainties also include the uncertainty due to variation of the groove depth at different locations of the sample.

Table 2 shows the example uncertainty budget. The components are assumed to be statistically independent.

The distribution of the cosine error related to the Y-tilt is chi-squared as the square of a normally distributed zero-mean variable. The X-tilt cosine error is written as gamma-distributed to account for the fact that this cosine error angle can be estimated from the measured profiles and corrected (not zero-mean distribution). Although the Y-tilt cosine error would also result theoretically in a correction due to the estimated uncertainty of a one-sided distribution of the squared zero-mean angle, with a non-zero mean this correction is probably better left undone, since the normally 'safe' over-estimation of uncertainty would lead to a significant error due to too large a correction. In this case, written for one of the profile measurements shown in figure 4, the X-tilt is very small.

Table 2. Uncertainty budget for step height/groove depth measurement for calibrating the Z scale.

Input parameter	Symbol	Estimate	Probability distribution	Standard uncertainty $u(x_i)$	Sensitivity coefficient	Uncertainty $u_i(h)$ (μm)
Left height	z_1	566.83 μm	Normal	<0.1 μm	0.5	0.05
Middle height	z_2	−540.85 μm	Normal	<0.1 μm	1	0.1
Right height	z_3	561.00 μm	Normal	<0.1 μm	0.5	0.05
Cosine error	β^2	6×10^{-8} rad^2	Gamma	10^{-6} rad^2	550 μm rad^{-2}	0.00055
Cosine error	γ^2	1.0×10^{-4} rad^2	$\chi 2$	1.4×10^{-4} rad^2	550 μm rad^{-2}	0.077
Temperature difference from 20 °C	Δt_{20}	0 °C	Rectangular	2.0 °C	0.012 μm °C^{-1}	0.024
Surface type	s	0 μm	Normal	0.1 μm	1	0.1
Repeatability	δ_{rep}	0 μm	Normal	0.05 μm	1	0.05
Measured height		1105.10 μm			Standard uncertainty	0.16
					Expanded uncertainty ($k = 2$)	0.31

3.2. X scale and resolution

For applications of the LCI sensor, lateral scale and resolution are important parameters, and in some cases the lateral resolution may be even more important than the highest possible accuracy in the lateral scale. Calibrated gratings with topography can be used for calibration and also essentially flat gratings with variations in reflectivity like Ronchi rulers. The latter perhaps captures best the general lateral magnification, while e.g. sinusoidal gratings with high amplitude may give slightly varying results due to surface type effects.

The X scale of the LCI1200 instrument was tested by measuring a commercial 3 μm-deep (i.e. relatively shallow) 800 μm-period square-wave etched silicon sample (calibrated with a traceably calibrated 2D optical coordinate measuring machine). The magnification of the X scale was measured based on the positions of the rising edges of the measured grating pattern. The magnification was measured at three different heights and lateral areas in all combinations, and the variation of magnification between different z and x areas was found to be less than 0.3%. This test was performed with a different LCI1200 head (same model, different serial number), which we had under test before the one used for all the other reported measurements.

A test using a calibrated Ronchi ruler with a 100 μm period, and analysis of the period of variation in the detected LCI intensity vector, indicated that the LCI X scale magnification error was less than 0.5%, but this can be further reduced by simple calibration if needed.

The X resolution was also measured with a commercial 3 μm-deep square-wave etched silicon grating sample with different grating periods. The 80 μm and 40 μm grating areas in the sample were still imaged with the full peak-to-peak amplitude, and the 20 μm grating suffered only a 30% attenuation (compare to the 5.5 μm pixel width). 8 μm and 4 μm gratings appeared almost flat, as could be expected. It seems that the instrument resolution is close to optimal for its pixel width.

The Y resolution was also tested simultaneously with the dynamic response as described in section 4.2, with a 100 μm-period grating, whereas the Y-curvature of the profile can be measured, e.g. by the linearity of the phase evolution of diagonally imaged Ronchi rulers. Based on initial tests, the curvature is less than a few micrometres.

Table 3. Z noise with different surfaces as the standard deviation of repeated profile measurements of a static sample. Unit is micrometres and each height and material is reported as the average of standard deviation, and the range of the per-pixel standard deviation values is written in parentheses.

z level	Clear polyester film	Printed silver on polyester	Optical mirror	Black silicon
+1300	0.42 (0.2–0.9)	0.13 (0.1–0.3)	0.25 (0.1–0.5)	
0	0.08 (0.05–0.13)	0.09 (0.05–0.15)	0.10 (0.04–0.18)	0.3
−1300	0.18 (0.08–0.30)	0.22 (0.15–0.30)	0.28 (0.08–0.80)	

4. Z noise and dynamic performance

4.1. Z noise with different materials

Noise in surface measuring instruments may be caused by environmental factors like vibration, or be intrinsic to the measurement instrument. Effects due to vibration of the sample can be essentially avoided in single profile-based snapshot measurements due to the short illumination and imaging time, freezing the motion.

Here we have measured the repeatability of single pixels with fixed in a virtually vibration-free environment. Table 3 shows the Z noise with different surfaces as the standard deviation of repeated single-shot profile measurements of a static sample at different heights. The number of repeats was 16.

The polyester film is a clear transparent plastic film for roll-to-roll production of printed electronics. Parts of the measurement area have printed silver conductors. The black silicon sample is micro/nanorough and has low reflectivity, of the order of 1%. Black silicon was only measured in the central z range before the sample was returned.

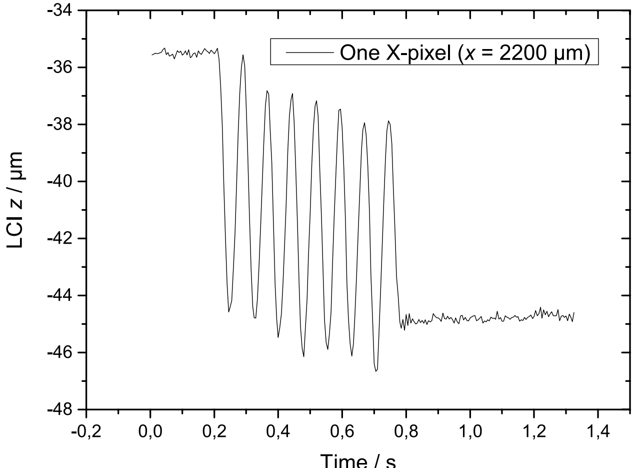

Figure 6. Profile from a Y-translated 100 μm period sinusoid grating. When the grating moves, a sinusoidal height variation is produced.

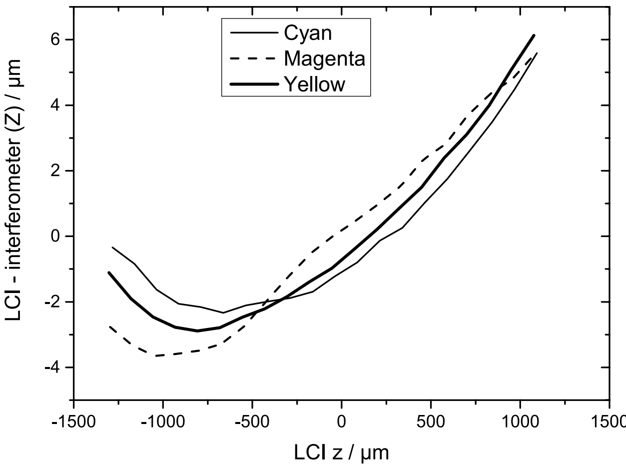

Figure 7. LCI z scale measured from different coloured areas of a commercial multicolour optical test sample.

Overall, the Z noise observed with the instrument can often be even at the 0.1 μm level, and rarely exceeds 0.3 μm rms.

The lighting intensity (pulse duration and sample effective reflectivity) of each X-pixel affects the noise level. The variations in noise level in different XZ areas may largely be attributed to the different distributions of LCI illumination intensity at different z levels. The pulse width was controlled during measurement at different heights, maintaining constant average intensity.

It should be noted that flatness error and calibration are different from per-pixel noise. The difference between different X-pixels when measuring, e.g. an optical flat can be somewhat larger than the noise in a single pixel in successive measurements when the sample is static, i.e. not moving or vibrating relative to the sensor.

4.2. Dynamic response, frame rate and motion freezing

When a line sensor is used, e.g. in such a dynamic setting where the sample is rapidly moving under the sensor, the dynamic response is an important characteristic describing the performance of the sensor in the sense of how it can measure rapid changes in topography. In the case of the LCI sensors, the successive profiles are supposed to be independently measured using separate pulses of light.

A test was developed to verify the dynamic capability of the LCI1200 sensor with a grating sample moving in the Y direction.

The frame rate used here is 200 Hz, or 200 frames per second (fps), with the full Z scale enabled (although not needed in this case). The sensor can measure up to 2500 fps with limited Z range and 500 fps with full range. However, since lighting pulse lengths of just 1–10 μs (microseconds) are suitable for many materials, each profile measurement can 'freeze motion' very well, and the profile is effectively captured over just a few microseconds. In this test, 27 μs light pulses were used. For materials with very low reflectivity, pulses of hundreds of μs are needed, even up to 1 ms.

Figure 6 shows a measurement from a single X-pixel when a 100 μm period grating is first static, then moving in the Y direction, then static again.

The fringe or ridge rate of the grating movement is approximately 12 grating periods/s, and the observed amplitude is similar to that seen in single instantaneous profiles when the ridges are oriented orthogonally to X, and similar to the amplitude measured from the sample with a tactile profilometer.

This shows that the successive profile measurements are independent, at least on this timescale, and that also the effective Y resolution or Y pixel size, describing the width of the area seen by each X pixel in the Y direction, is adequate for this grating period to be imaged without an apparent magnitude decrease caused by Y averaging.

Testing and verifying the motion freeze, pulse width and frequency, and frequency stability could be done, e.g. by measuring choppers or loudspeakers synchronized with or driven by reference frequencies, or with a photodetector to measure the illumination pulses.

5. Effect of surface colour, slope and specularity on the LCI *Z* scale

5.1. Sample colour and Z scale

Changes in sample reflectivity as function of wavelength could theoretically cause changes in the Z scale of the chromatic instrument. To measure the Z-scale magnification and linearity with different colours, a commercial multicolour sample was used.

Figure 7 shows the measured LCI versus laser interferometer curves for the cyan, magenta and yellow areas of a commercial matte optical multicolour test sample (Pico ColorChecker/ColorGauge Pico, from Edmund Optics, by Image Science Associates). Small changes in the difference between the yellow and magenta areas occurs possibly where the wavelengths corresponding to the measured height become short enough that the intensity of scattered light from the focus point is relatively lower in the magenta than in the yellow

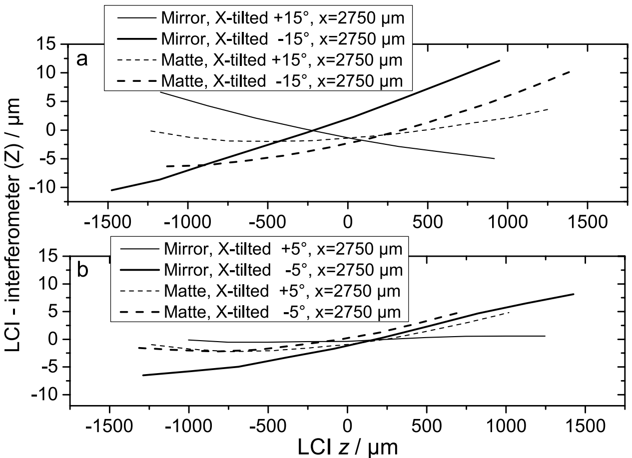

Figure 8. *X*-tilted matte and specular samples; resulting *Z* scale measured at $x = 2750$ μm.

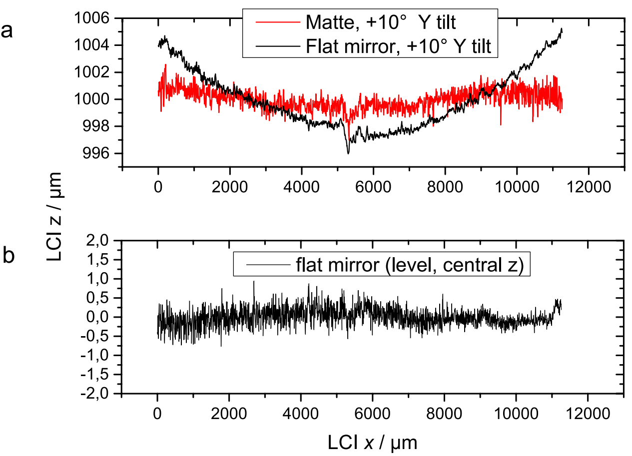

Figure 9. Matte sample and flat mirror tilted at +10°, imaged at approximately +1000 μm height. The specular flat mirror appears slightly curved (a). Flat mirror at level orientation and central height (b) linear fits have been subtracted from the data in this figure to show nonlinear behaviour and to overlap the data. Approximate mean height levels are preserved. Note the different vertical scale magnifications.

area. It could be assumed that the wavelength-dependent reflectivity of the sample biases the spectral peak detection-based *z* scale by a small amount. However, the effect of surface colour in this test is small. The rms difference between yellow and magenta is 0.69 μm and between yellow and cyan 0.46 μm. This test measured the scales individually for each colour, comparing gain and nonlinearity, whereas later in section 5.3 a test result with an approximately flat heterogeneous sample is presented to further verify possible offset issues of heterogeneous samples.

5.2. Specularity and surface slope, effect on Z scale magnification

Effect of surface slope angles proved to be an important factor in the characterization, and the effect was dependent on the surface specularity. In order to characterize the effect of sloped surfaces on the *Z* scale, a mirror sample and matte sample were measured in the interferometrically tracked movable sample setup.

Figure 8 shows the *Z* scale measurement results with flat samples for different *X*-tilt angles and specular versus matte samples. The specularity and slope are interrelated, since the main effects related to surface specularity seem to occur only on slopes (and mostly in peripheral measurement areas). The specular flat was an optical mirror, and the non-specular sample was a commercial protected silver-coated ground-glass diffuse reflector (DG10-600-P01 and DG10-1500-P01 from Thorlabs). The sample angle was adjusted using the goniometer stages in the sample holder.

It is clear that in the off-central *X* area ($x = 2750$ μm), the specular tilted surface is imaged with slightly varying scale amplification depending on the tilt angle, and also that with the matte sample the *Z* scale results differ depending on the angle but much less so than with the specular surface. With the matte surface and ±5° tilt the differences are of the order of 1–2 μm or 0.1%, but with specular surface at ±15° surface angles the differences are larger, resulting in *Z* scale amplification differences of 1–2%.

The graphs shown are for $x = 2750$ μm. Each curve has been individually set at zero mean, so constant *Z* offsets between the curves are arbitrary.

At $x = 8250$ μm, i.e. on the opposite side of the centre of the *X* range at ~5600 μm (pixel 1024), the *Z*-scale deviations from the level-surface situation are of the opposite sign but of similar magnitude and form, and generally the longer the *X* distance is from the middle, the faster the difference in *z* scale between different sample surface angles grows. In the central *X* range, the differences in the *Z* scales are small.

Figure 9 shows matte and flat mirror samples measured at a 10° tilt in the *Y* direction, imaged at high *Z* offset (9(a)). The mirror measurement shows a slightly curved shape, presumably due to similar small *X*-dependent differences in the *Z* scale for a tilted specular surface. Figure 9(b) shows the flat mirror measured at level orientation (and zero *Z* offset).

A rather natural explanation or expectation is that compared to the mirror reflection, the non-specular sample surface reduces the surface angle dependent effects since, by definition, a fully non-specular surface scatters light in all directions, independent of the incident light angle.

Furthermore, the LCI *Z* scale was also measured with the polyester and printed silver sample. The scale in both areas, plain clear polyester and printed silver coating, was similar to the corresponding mirror and matte scales (with small tilt) shown previously, within 1–2 μm.

5.3. Heterogeneous samples for measuring Z scale offset effects

In order to characterize the possible *Z* scale offset-like differences caused by different materials and slope angles, suitable samples and methods were developed. Tests were made using sinusoid grooved gratings with specular and etched (matte, micro-/nanorough) metal surfaces, and a Teflon surface partly

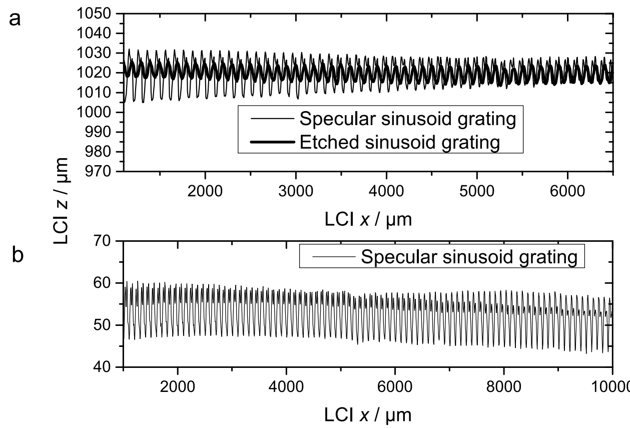
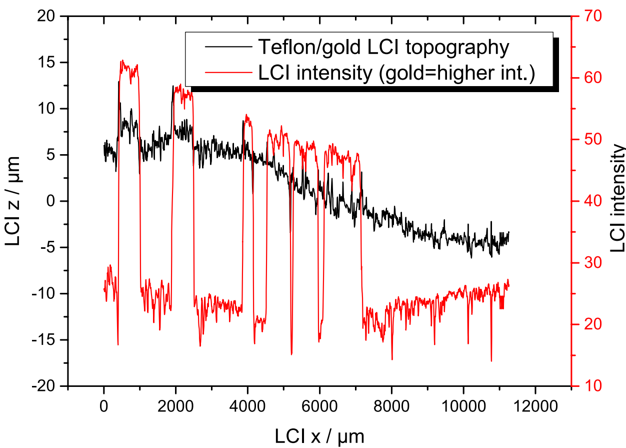

Figure 10. Specular and matte sinusoid gratings imaged with LCI1200; specular and matte grating shown at high Z offset (a), and specular grating in the central Z area. All graphs are raw data. Note the different scales in the two plots.

Figure 11. Gold leaf attached to parts of a slightly rough and wavy Teflon surface.

covered with gold leaf. The sinusoid sample presents varying surface slopes in the same surface, and the Teflon and gold leaf have highly different optical properties.

The gratings are made of grooved metal and have 8–10 μm peak-to-peak amplitude. The specular grating imaged at high Z offset in figure 10(a) has too high an apparent amplitude in the peripheral XZ area, presumably due to the strongly varying slope angles of the waveform. This is mostly explained by the gain variation with surface angle with specular surfaces. The acid-treated metal sinusoid grating with a non-specular surface has uniform apparent amplitude in the same conditions. In figure 10(b), the specular metal sinusoid grating imaged with a small Z offset (in contrast to the large offset in figure 10(a)) still has slightly too high an amplitude in the central Z range in the peripheral X areas, but in the centre the amplitude is close to the 10 μm peak-to-peak value. The sloped sides of the sinusoid grooves in these samples correspond to roughly $\pm 15°$ angles.

The Teflon/gold sample was made in order to have an approximately flat surface with highly different optical properties in the same sample area. The slightly curved and rough Teflon piece, after attempts at polishing it, was covered with gold leaf, slight pressure was applied with a cloth/finger, and the pressure was removed. The somewhat distorted gold leaf (thickness approximately 0.1 μm) stuck to parts of the Teflon surface. Figure 11 shows the resulting profile and detected light intensity from the same measurement line. Teflon scatters light from within the material and also from the surface (reflection), whereas the gold surface has mainly a highly specular reflection from the surface. The measured profile shown with the LCI intensity vector in figure 11 seems to be of roughly the same height in the high-intensity gold-covered parts as in the lower-intensity bare Teflon parts. Some possible edge effects and intensity-correlated Z offset differences seem to occur, especially at the highest detector intensities. The topography peaks could also be true topographical features. The effect of very different optical properties seems to be small in this case, especially by comparison with the instrument's full Z scale.

6. Discussion

The developed methods are also applicable to other optical measurement instruments, depending on the type of instrument. Other line-type optical sensors could be characterized in a similar way, and also point-type sensors can be characterized with different surface angles and types.

In the case of the LCI instrument tested here, beyond calibration and checking of instrument properties, developments to the sensor or ways of further enhancing accuracy could be envisaged.

With the high resolution and repeatability of the LCI1200 instrument, if very high absolute accuracy is needed with surface types that affect the Z scale the most, calibrations could be done with specific illumination, sample material and/or tilt angle, to apply specific corrections or calibration functions/tables for a certain task.

Generally, it could be difficult to detect the sample slope, specularity, reflectivity etc to a useful degree for applying new corrections without extra sensors or information on the sample material measured. On the other hand, for most applications, a single Z-scale calibration for all samples is probably enough with the LCI1200.

Also, we note here that specularity and surface slope also depend on the size scale one is looking at. A sample material that is matte and linearly sloped on a bigger scale might be specular but wrinkly on another, leading to different effective specularity when viewed with instruments using different pixel size.

7. Conclusion

In this work, methods were developed for the measurement of the metrological characteristics of optical topography instruments, especially line confocal chromatic sensors.

A Z (depth) calibration and checking method using one groove depth sample was developed and verified with laser interferometry-based instrument calibration. Uncertainty analysis related to groove depth/step height-based Z calibration was presented. The Z scale in different X areas was also

measured against the laser interferometer. The results show that a groove sample can be used to attain better than 1/1000, or sub-micron, Z-scale accuracy in the case of the LCI1200 sensor. The X scale and resolution, dynamic performance and Z noise of the LCI1200 sensor were also tested using gratings and different sample materials.

The effect of different surface parameters including colour, specularity, and slope angle on the Z scale was characterized with coloured, matte and mirror samples and laser interferometry, and generally the effect of colour was minor. Matte (non-specular) surfaces had a relatively uniform Z scale at different X positions, even for highly sloped surfaces. In the extreme case of combining a specular surface, steep slope, and peripheral area in the XZ measurement range, the related Z scale amplification variations were of the order of 1%. Overall, the performance of the LCI1200 sensor was found to be as good as a fast, optical, versatile topography instrument.

Acknowledgments

This work forms part of the EMPIR project MetHPM [14]. The EMPIR initiative is co-funded by the European Union's Research and Innovation Programme and the EMPIR Participating States.

ORCID iDs

Jeremias Seppä https://orcid.org/0000-0002-6781-8443
Antti Lassila https://orcid.org/0000-0002-6991-7082

References

[1] Leach R 2011 *Optical Measurement of Surface Topography* (Berlin: Springer)
[2] Giusca C L, Leach R K and Helery F 2012 Calibration of the scales of areal surface topography measuring instruments: part 2—amplification coefficient, linearity and squareness *Meas. Sci. Technol.* **23** 065005
[3] Leach R *et al* 2015 Open questions in surface topography measurement: a roadmap *Surf. Topogr.: Metrol. Prop.* **3** 013001
[4] Garnaes J, Kühle A, Nielsen L and Borsetto F 2005 True three-dimensional calibration of closed loop scanning probe microscope *Nanoscale Calibration Standards and Methods: Dimensional and Related Measurements in the Micro- and Nanometer Range* ed G Wilkening and L Koenders (New York: Wiley) pp 193–204
[5] Korpelainen V and Lassila A 2007 Calibration of a commercial AFM: traceability for a coordinate system *Meas. Sci. Technol.* **18** 395–403
[6] Cha S, Lin P C, Zhu L, Sun P C and Fainman Y 2000 Nontranslational three-dimensional profilometry by chromatic confocal microscopy with dynamically configurable micromirror scanning *Appl. Opt.* **39** 2605–13
[7] Ruprecht A K, Wiesendanger T F and Tiziani H J 2004 Chromatic confocal microscopy with a finite pinhole size *Opt. Lett.* **29** 2130
[8] Hillenbrand M, Weiss R, Endrödy C, Grewe A, Hoffmann M and Sinzinger S 2015 Chromatic confocal matrix sensor with actuated pinhole arrays *Appl. Opt.* **54** 4927–36
[9] ISO 25178 part 602 2010 *Geometrical product specification (GPS)—Surface texture: Areal—Part 602: Nominal characteristics of non-contact (confocal chromatic probe) Instruments* (Geneva: International Organization for Standardization)
[10] Nouira H, El-Hayek N, Yuan X, Anwer N and Salgado J 2014 Metrological characterization of optical confocal sensors measurements (20 and 350 travel ranges) *J. Phys.: Conf. Ser.* **483** 012015
[11] Focalspec 2018 http://focalspec.com (Accessed: 18 December 2017)
[12] ISO 5436 part 1 2000 *Geometrical Product Specification (GPS)—Surface Texture: Profile Method Measurement Standards—Material Measures* (International Organization of Standardization)
[13] JCGM 100:2008 *Evaluation of Measurement Data—Guide to the Expression of Uncertainty in Measurement* (Geneva: International Organization for Standardization) http://bipm.org/utils/common/documents/jcgm/JCGM_100_2008_E.pdf
[14] EMPIR 2018 14IND09 MetHPM project webpage http://empir.npl.co.uk/MetHPM (Accessed: 21 December 2017)